



CAUSALITY CORRELATION IN AEROACOUSTIC EXPERIMENTS BY MEANS OF SIMULTANEOUS PIV AND MICROPHONE-ARRAY MEASUREMENTS

Arne Henning

Technical University of Berlin,

Institute for Aero- and Astronautics (ILR),

Berlin, Germany. Current address: German Aerospace Center (DLR), Göttingen, Germany

Lars Koop and Klaus Ehrenfried

German Aerospace Center (DLR),

Göttingen, Germany

ABSTRACT

In this paper we present applications of the causality correlation technique by means of simultaneous PIV measurements in a turbulent flow and microphone-array measurements in the aeroacoustic far field. Both measurements are conducted in a synchronized manner so as to enable the calculation of the cross-correlation between the acoustic pressure and flow quantities derived from the measured velocity fluctuations. The main idea of the concept presented here is to use the therewith obtained coefficient matrix to identify regularities in the flow that are related to the radiated sound field. Here we show a comparative study of the results for measurements on different flow-configurations with strong tonal components as well as with broadband spectra in the acoustic far-field.

1 INTRODUCTION

Acoustic mirrors and phased microphone arrays are standard tools used to localize and quantify aeroacoustic sources. But measurements in the far field don't give any direct information about the source processes occurring in the near field, whereas measurements in the near field, although able to deliver information about the structures and the dynamics of the involved flow, are nevertheless very difficult to analyze in terms of an estimation of the radiated far-field sound. One way around this is the simultaneous measurement of the acoustic pressure in the far-field together with some other near-field quantity. In this manner the far-field pressure can be correlated

with the near-field quantity to identify aeroacoustic sources. The simultaneous measurement of acoustic pressure fluctuations in the far-field of a turbulent flow together with a near-field quantity has been investigated by various authors in the past [2, 6, 12]. In this manner the far-field pressure can be correlated with the near-field quantity to identify flow structures which are related to the aeroacoustic source mechanism. Rackl [8] introduced the name "causality correlation" for this correlation approach. Previous experiments [3, 4] have shown that synchronized PIV and microphone measurements can be used to obtain the cross-correlation function between a near-field quantity and the acoustic pressure in the far-field. These measurements described here have been performed on different flow configurations, namely a cylinder-wake and a rod-airfoil configuration. The advantage of using Particle Image Velocimetry (PIV) for measuring the near field quantity is the non-intrusive determination of the instantaneous flow velocity in a region instantaneously.

1.1 Causality Correlation

In the investigations presented here, the correlation-coefficient $R_{\phi,p}$ between the near-field quantity ϕ measured via PIV and the acoustic pressure p is calculated in the time domain by an ensemble average over a certain number of PIV snapshots. The recording rate of the used PIV systems is in the order of 1 Hz. Clearly, this rate is too slow to capture the temporal development of an unsteady flow field in most practical applications in the field of aeroacoustics. But the low recording rate assures that the PIV measurements are statistically independent, which implies a maximum suppression of uncorrelated parts of the measured quantities per PIV snapshot during the calculation of $R_{\phi,p}$.

The normalized cross correlation $R_{\phi,p}(\mathbf{x}, \mathbf{y}, \tau)$ is defined as:

$$R_{\phi,p}(\mathbf{x}, \mathbf{y}, \tau) = \frac{S_{\phi,p}(\mathbf{x}, \mathbf{y}, \tau)}{\sigma_{\phi}(\mathbf{x}) \sigma_p(\mathbf{y})} = \frac{\langle \phi'(\mathbf{x}, t) p'(\mathbf{y}, t + \tau) \rangle}{\sqrt{\langle \phi'^2(\mathbf{x}, t) \rangle \langle p'^2(\mathbf{y}, t) \rangle}}, \quad (1)$$

where $\phi(\mathbf{x}, t)$ represents a near-field quantity measured at position \mathbf{x} and time t . The variable τ is the time shift between the pressure signal p at the position \mathbf{y} and the point in time the quantity ϕ is obtained. The cross correlation $S_{\phi,p}(\mathbf{x}, \mathbf{y}, \tau)$ is normalized by the root-mean-square (RMS) values of the fluctuations ϕ' and p' which are denoted by $\sigma_{\phi}(\mathbf{x})$ and $\sigma_p(\mathbf{y})$. In the present experiments the flow field is recorded by the PIV system at discrete times t_n and the near-field quantity is evaluated from these recordings. The time between the PIV measurements is large enough so that the individual images can be considered as statistically independent. The far-field pressure is recorded at discrete times¹ simultaneously to the flow field measurements, but using a much higher sampling rate than with PIV. The system clock of the PIV system has been synchronized with the data-acquisition system used for the acoustic pressure. Then the cross correlation between the near-field quantity and the acoustic pressure can be calculated in a discrete manner using:

$$S_{\phi,p}(\mathbf{x}, \mathbf{y}, \tau) = \frac{1}{N} \sum_{n=1}^N [\phi'(\mathbf{x}, t_n) p'(\mathbf{y}, t_n + \tau)]. \quad (2)$$

¹In the following $\tau \in k/f_p$ with $k = 1, 2, 3, \dots, K$, where K is the total number of pressure samples recorded.

where N is the number of PIV measurements. The RMS-value of the near-field quantity, which is required for normalization, can be calculated from the measured data by:

$$\sigma_\phi(\mathbf{x}) = \sqrt{\frac{1}{N} \sum_{n=1}^N \phi'^2(\mathbf{x}, t_n)} \quad \text{und} \quad \sigma_p(\mathbf{y}) = \sqrt{\langle p'^2(\mathbf{y}) \rangle}. \quad (3)$$

The averaging for the standard deviation $\sigma_p(\mathbf{y})$ is carried out over all recorded pressure samples. The number of these samples is typically several orders of magnitude higher than N . It should be noted here that the critical parameter is the number of PIV recordings N . If N is too low, uncorrelated parts of the measured quantities cannot be sufficiently suppressed. This results in a high noise level in the resulting cross-correlation $S_{\phi,p}$. The definition of a sufficient number of recordings may of course depend strongly on the particular case under consideration. In case of simultaneous microphone measurements at different locations \mathbf{y}_m in the far field (e.g. using a microphone-array), the correlation of ϕ with the delayed and summed up pressure signals p_f reads:

$$\begin{aligned} S_{\phi,p_f}(\mathbf{x}, \mathbf{x}_q, \tau) &= \frac{1}{N} \sum_{n=1}^N [\phi'(\mathbf{x}, t_n) p_f(\mathbf{x}_q, t_n + \tau)] , \\ &= \frac{1}{N} \sum_{n=1}^N \left[\phi'(\mathbf{x}, t_n) \sum_{m=1}^M w_m p(\mathbf{y}_m, t_n - \tau_{mq} + \tau) \right] . \end{aligned}$$

Here w_m is an appropriate weighting factor for each microphone signal, \mathbf{x}_q is a chosen point in the flow field and $\tau_{mq} = |\mathbf{y}_m - \mathbf{x}_q|/c_0$ is the travel time from \mathbf{x}_q to \mathbf{y}_m with the speed of sound c_0 . After rearranging one obtains:

$$\begin{aligned} S_{\phi,p_f}(\mathbf{x}, \mathbf{x}_q, \tau) &= \sum_{m=1}^M \left[\frac{1}{N} \sum_{n=1}^N \phi'(\mathbf{x}, t_n) w_m p(\mathbf{y}_m, t_n - \tau_{mq} + \tau) \right] , \\ &= \sum_{m=1}^M [w_m S_{\phi,p}(\mathbf{x}, \mathbf{y}_m, \tau - \tau_{mq})] . \end{aligned} \quad (4)$$

Thus, the summation of the time-shifted and weighted correlation functions is equivalent to a direct calculation of the correlation function between the delayed and summed up pressure signals with the near-field quantity ϕ . The advantage of using Eq. (4) is that the computation time for the summations over m is comparatively small, once the correlation functions for all microphones are calculated². Note that in the investigation presented here, the cross-correlation coefficient is the major objective. Therefore $S_{\phi,p_f}(\mathbf{x}, \mathbf{x}_q, \tau)$ needs to be normalized by σ_ϕ and σ_{p_f} . But assuming ergodicity, σ_{p_f} can be calculated from a reduced number of pressure samples, resulting in a negligible computation time.

²The number of microphones M is usually small compared to the number of recorded PIV samples N .

2 EXPERIMENTS

in a first step, the flow configuration of a cylinder wake has been investigated in a closed test-section. Figure 1 shows a schematic setup and a picture of the configuration. The experiments

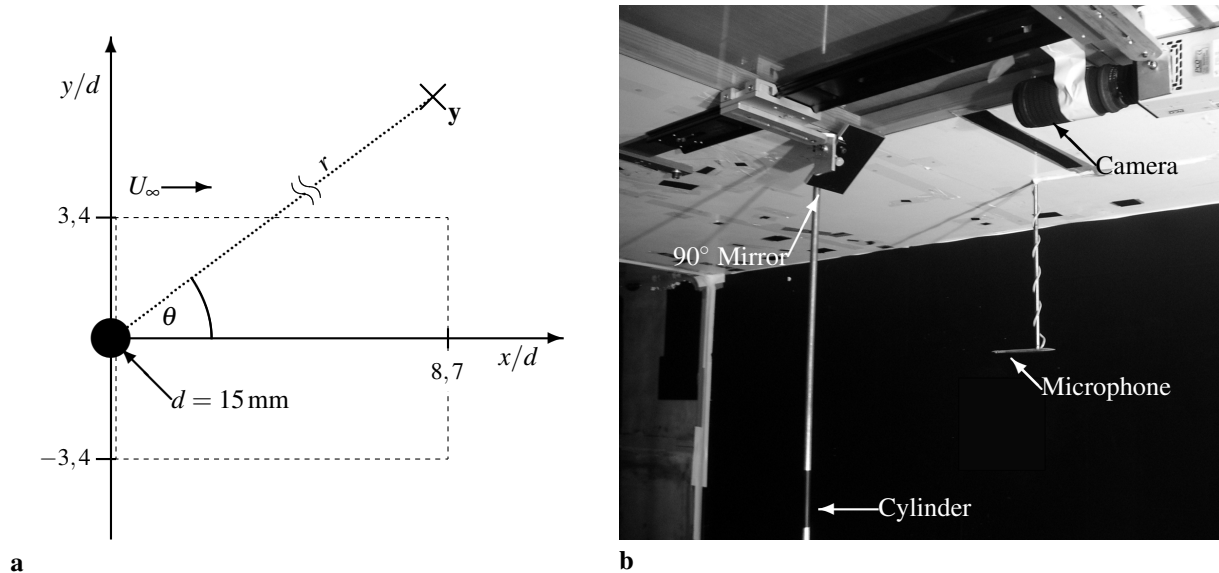


Figure 1: PIV and microphone measurement of a cylinder wake flow. **a:** Schematic setup of the experiment. The dashed square indicates the PIV field of view. **b:** Picture of the experimental setup. The PIV camera is mounted on the wind tunnel ceiling and records particle images via an mirror located upstream.

are conducted in the $2.0 \times 1.4 \text{ m}^2$ Göttingen type wind tunnel with a closed test section and reverberant side walls. The Reynolds-number is $Re = 19000$ based on a cylinder diameter of $d = 15 \text{ mm}$ and a free stream velocity $U_\infty = 20.55 \text{ m/s}$. The microphone is laterally shifted at an angle of $\theta = 51^\circ$ at a distance $r/d = 42.7$ to the cylinder. The sampling rate for the pressure signal is $f_p = 102.4 \text{ kHz}$. Velocity data are acquired with a 2D-2C PIV system at $f_s = 2.5 \text{ Hz}$. In a next step the correlation technique has been applied to a rod-airfoil flow configuration by means of simultaneous microphone-array and PIV measurements [4]. In such a configuration the airfoil undergoes a broadband perturbation dominated by the turbulent periodic shedding frequency of the vortex separating from the rod. Compared to the flow field generated by a single cylinder, the radiated noise is spread over a wider range of frequencies. The outline of the experimental setup is depicted in Fig. 2. Experiments were conducted in an aeroacoustic open-jet, closed-circuit wind tunnel at $Re_c = 500000$ based on a chord-length of $c = 150 \text{ mm}$ and a free stream velocity $U_\infty = 50 \text{ m/s}$. The span of the configuration is $s = 800 \text{ mm}$. For all measurements presented here the cylinder is shifted to $y_{rod}/c = 6.5 \text{ mm}$, in order to include an almost turbulence free section in a lower region of interest. A number of 87 microphones are arranged in the plane $y/c = 8$ at positions depicted in Fig. 2 c ($f_p = 50 \text{ kHz}$). A coplanar multi-plane PIV system has been used ($f_s = 0.7 \text{ Hz}$), providing statistically independent samples of the temporal derivative of the velocity vector-field.

In a more recent investigation the correlation technique is tested on a broadband aeroacoustic

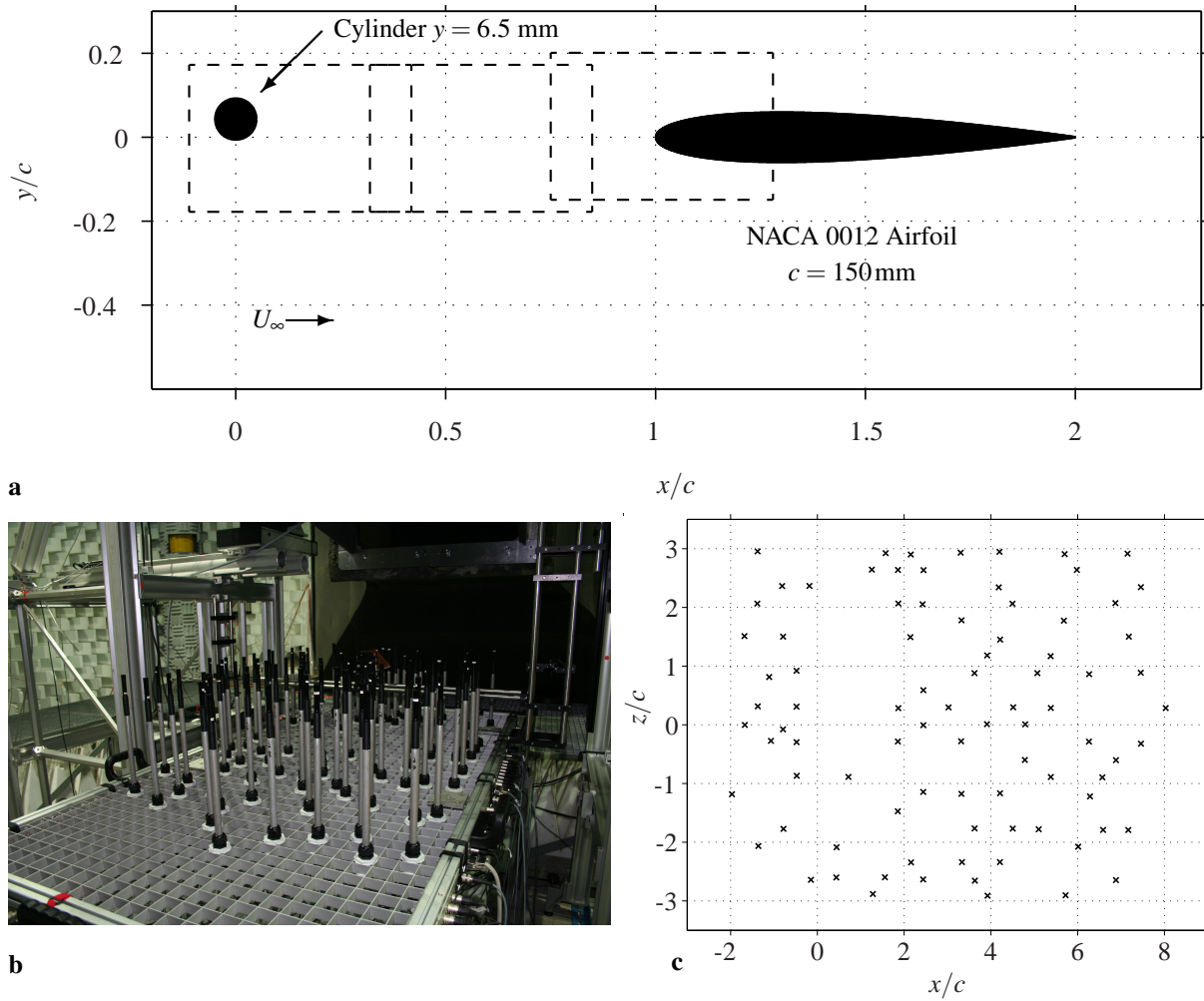


Figure 2: PIV and microphone-array measurement of a rod-airfoil configuration. **a**: Schematic setup of the experiment. The dashed squares indicate the PIV fields of view. **b**: Picture of the used microphone-array. 87 microphones are arranged in the plane $y/c = 8$ at positions depicted in **c**.

source. The flow inside a jet was chosen because a variety of experimental results are available for comparison [7, 10, 11]. Measurements have been performed on a cold jet in the region of the potential core at three different Mach numbers $Ma = 0.5$, $Ma = 0.7$ and $Ma = 0.9$. The cold jet was generated by a 15 mm diameter (D) nozzle mounted on a settling chamber of 200 mm in diameter and approximately 0.5 m in length. A number of 10 microphones ($f_p = 50$ kHz) are arranged at different distances r to the nozzle exit and different angles θ between the jet axis and the direction of observation (see Table 1). In order to obtain all three velocity components in a plane, a 2D-3C Stereo-PIV system is used in two different fields of view as shown in Fig. 3. The setup in this experiment was chosen to allow a proof of concept of the presented correlation technique and is not optimized for the aeroacoustic investigation of the jet-flow field itself. For example the test-facility is not anechoic. Acoustic absorbent material was placed around the vicinity of the nozzle only and not at the ceiling and walls of the room.

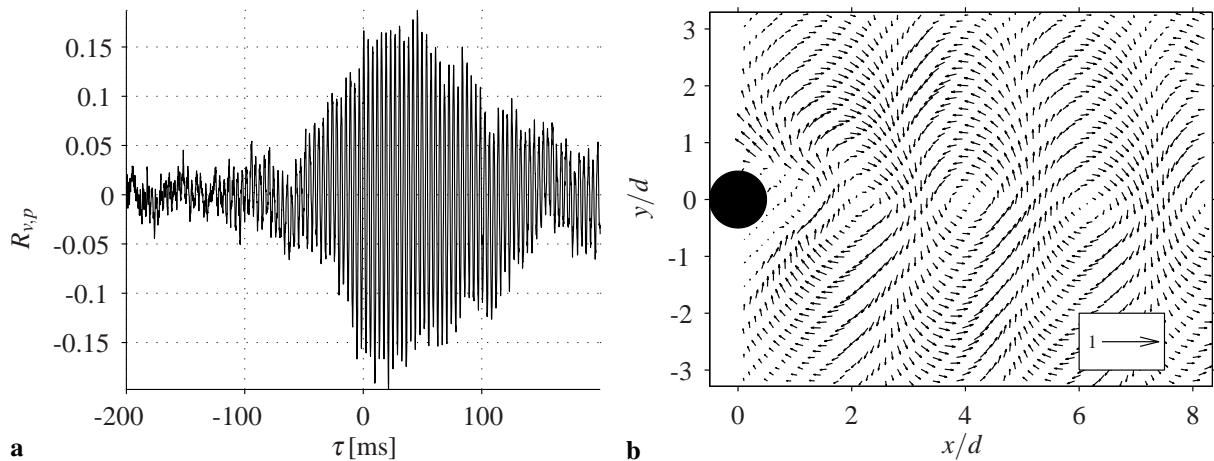


Figure 4: **a**: The temporal evolution $R_{v,p}$ at $[x/d; y/d] = [1.6; 0.55]$. **b**: Instantaneous distribution of $(R_{u,p}, R_{v,p})$ depicted as a vector plot for $\tau = 1$ ms.

The observed results are very different from those we present in section 3.2 for the correlation function between the acoustic pressure and the velocity fluctuation in a jet. In the case of a jet, typically the correlation function shows only a relatively short event which consists mainly of a single positive and negative deflection. The regular oscillations of $R_{v,p}$ in the present result can be explained by the strong coherence of the periodic structures in the flow field, illustrated by the cross-correlation $R_{v,v}$ at $[x/d; y/d] = [1; 0]$ depicted in Fig. 5 **b**. The structures generate a sound field with the same periodicity, which is perceived as tone. Hence, the correlation between the velocity fluctuations and the acoustic pressure shows the same oscillations as the input signals. The larger temporal coherence of both signals leads also to a significant correlation at negative τ values. This is also observed by [1] for the correlation between the velocity at two different positions in the cylinder wake. The specific shape of the envelope of the plot $R_{v,p}$ as a function of τ can be explained by reflections at the side walls of the test section, which have a strong influence on the microphone signal as can be seen from the envelope of the autocorrelation-function $R_{p,p}$ depicted in Fig. 5 **a**. Without reflections one would expect the maximum amplitude of the correlation function at a value $\tau_0 = r/c_0$ which matches with the travel time directly from the cylinder to the microphone. But in the present experiment multiple reflected signals are also received by the microphone and contribute to the correlation function at larger positive delay times τ , which correspond to travel distances of several times the channel width. A complicated interference of the directly emitted and the reflected waves takes place in the test section, and the superimposed waves interact constructively and destructively. Depending on the coherence length in the flow and the position of the microphone, the maximum amplitude of the correlation function can be shifted towards larger τ values, as is observed here. The delay time of $\tau = 0.025$ s is equivalent to a travel distance of about 8 m. This shift cannot be attributed to the larger sound travel time from the cylinder to the microphones, since this difference would be of the order of 10^{-5} s. Thus, in the present case the correlation function is clearly dominated by reflected waves.

The widespread distribution of $R_{v,p}$ is depicted in Fig. 6 **a** for $\tau = 1$ ms. Figure 6 **b** shows the temporal evolution of the normalized correlations $R_{v,p}$ along the axis $y/d = 0.85$. The solid

line represents the propagation time τ_p of the flow structures with the time averaged velocity $U(x) = \langle u(x) \rangle$ along the axis with $\tau_p(x) = (-x)/U(x) + r/c_0$. It can be seen, that for $x/d > 1$ the phase shift of $R_{v,p}$ corresponds to the group velocity $U(x)$ of the flow structures traveling the downstream distance x from the rod, and cannot be attributed to the larger sound travel time from the locations \mathbf{x} to the microphone.

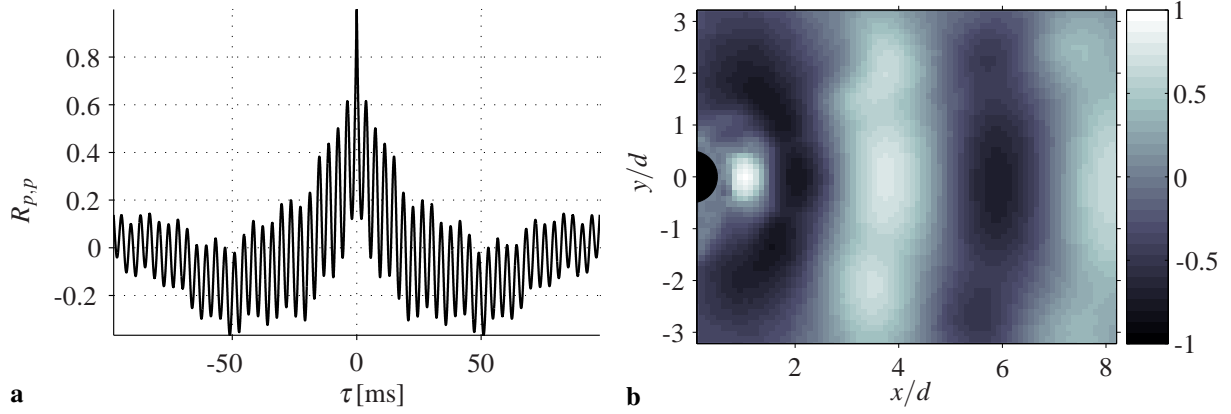


Figure 5: **a:** Autocorrelation-function $R_{p,p}$ of the pressure fluctuations p . **b:** Spatial distribution $R_{v,v}$ at $[x/d; y/d] = [1; 0]$.

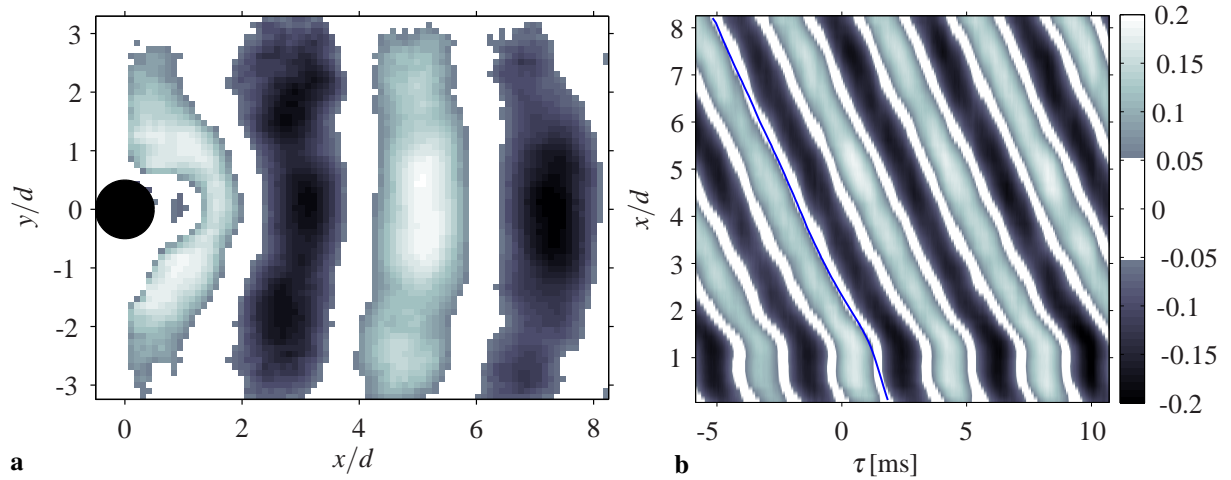


Figure 6: **a:** Spatial distribution of $R_{v,p}$ for $\tau = 1$ ms. Temporal evolution of $R_{v,p}$ along the axis $y/d = 0.85$. **b:** The solid line depicts $\tau_p(x) = (-x)/U(x) + r/c_0$.

3.2 Rod-Airfoil

Unless otherwise specified, the following results have been obtained from the configuration with $U_\infty = 50$ m/s. The axes in the figures are scaled to the chord-length c . x and y are local coordinates in the measurement plane with the origin at the cylinder axis for $y_{rod}/c = 0$. The

x -axis points in the mean flow direction. Some fields of view include areas of missing vectors corresponding to shadow zones of the laser light-sheet. The spatial resolution of the PIV measurement is 0.94 mm in the x - and y direction (interrogation-window size: 48 px \times 48 px; 50% overlap). The thickness of the lightsheet is approx. 1 mm. A number of 5000 PIV snapshots are considered for the calculation of the cross-correlation. The cross-correlation coefficient is calculated using Eq. (4) using the signals of all 87 microphones.

The temporal evolution of the cross-correlation coefficient $R_{v,p}$ at position $[x/c; y/c] = [0.98; 0]$ is plotted in Fig. 7 **a**. The coefficient fluctuates over time in a sine-type oscillation with maxi-

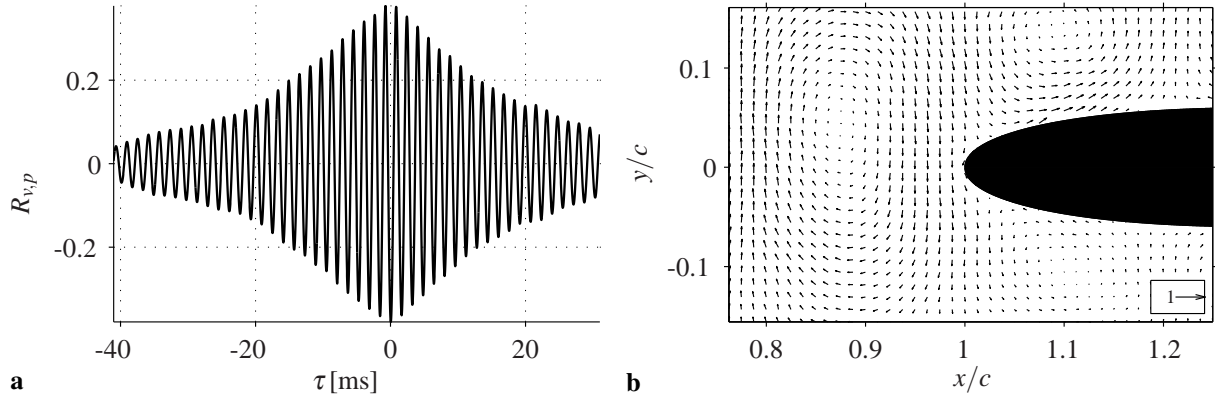


Figure 7: **a**: The temporal evolution of the cross-correlation coefficient $R_{v,p}$ at position $[x/c; y/c] = [0.98; 0]$. **b**: The instantaneous distribution of the cross-correlation coefficient $[R_{u,p}, R_{v,p}]$ for $\tau = 0$ ms depicted as a vector plot.

imum values of about $|R_{v,p}| = 0.3$. The envelope of $R_{v,p}$ as a function of τ shows no skewness and the distribution is symmetric around a maximum, located at $\tau = 0$ ms. This results differ significantly from findings in section 3.1, where the rod is installed in a closed test section with reverberant side walls. Therein, a shift of the correlation coefficient towards larger τ values is observed, not matching the sound travel time directly from the cylinder to the installed in-flow microphone. This difference in shape as well as the larger kurtosis of the envelope has been assigned to the dominance of the reflected waves from the side walls. This is not the case in the present investigation where strong reflections are damped by the anechoic chamber. The fundamental difference of the sound field can be seen by comparing the autocorrelation functions of p depicted in Fig. 7 **a** and 5 **a** (section 3.1). Both figures are also illustrating the strong coherence of the pressure fluctuations and therewith the need for a low sampling frequency in order to obtain statistically independent PIV snapshots. Fig. 7 **b** shows the instantaneous distribution of the cross-correlation coefficient $[R_{u,p}, R_{v,p}]$ for $\tau = 0$ ms depicted as a vector plot. Vortical structures split at the leading edge and stretch along the airfoil. The resulting pattern has a strong similarity to the first POD modes, satisfactorily describing the vortex-airfoil interaction (see Jacob et al. [5] and references therein). The results in section 3.1 have already indicated that the correlation technique functions as a extraction of the most energetic structures in the flow, which are responsible for the sound generating process.

Figure 9 shows the spatial distribution of $R_{v,p}$ in the region between the rod and the airfoil for $\tau = 0$. The sign of $R_{v,p}$ alternates between positive and negative values downstream of the

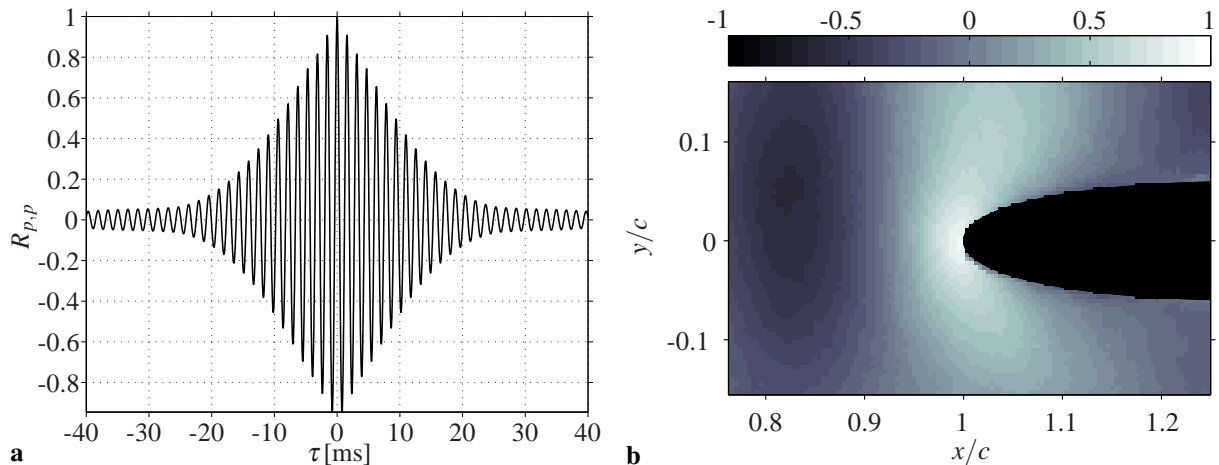


Figure 8: **a:** The autocorrelation-function $R_{p,p}$ where p is the pressure fluctuation from a single microphone at $\mathbf{y}_m = [x/c; y/c; z/c] = [5.7; -8; 0.9]$. **b:** The cross-correlation $R_{v,v}$ at $[x/d; y/d] = [1; 0]$.

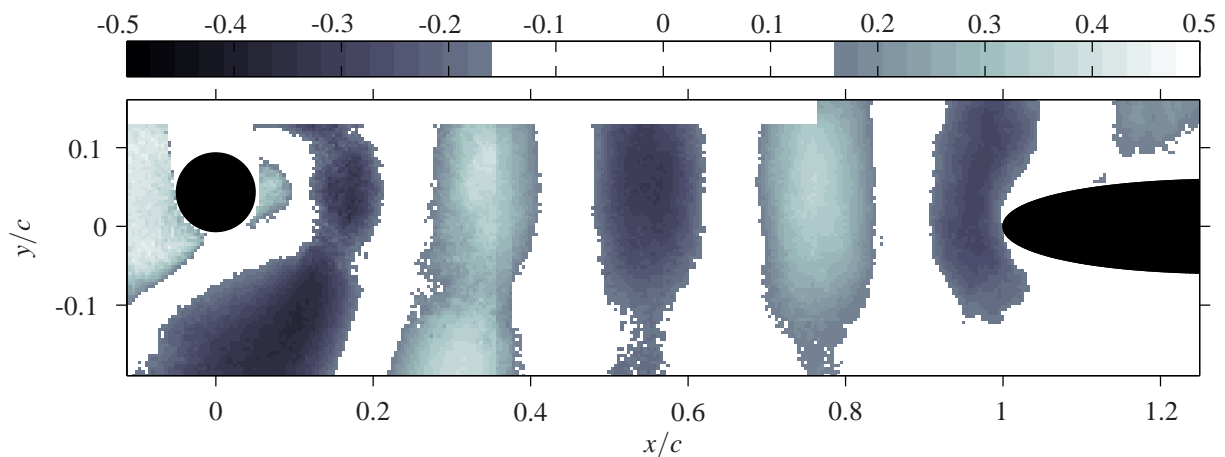


Figure 9: Spatial distribution of $R_{v,p}$ in the region between the rod and the airfoil for $\tau = 0$.

cylinder and the values are maximal in the near-wake of the cylinder and not at the airfoil LE. This is remarkable, since the leading edge is suspected to be the main aeroacoustic source region. But the flow structures become less periodic with increasing downstream distance from the rod and most likely more three dimensional. Therefore and because of the resulting higher noise level of v' and u' in the LE region, a lower correlation coefficient is observed in this area. It will be shown in the following that the temporal evolution of $R_{v,p}$ with τ supports this explanation; and that the main source region can indeed be attributed to the leading edge of the airfoil by means of the correlation technique presented here. Figure 10 shows the temporal evolution of the normalized correlations $R_{v,p}$ along the axis $y/c = 0$. The solid line represents the propagation time τ_p of the flow structures with the time averaged velocity $U(x) = \langle u(x) \rangle$ along the axis with $\tau_p(x) = (\mathbf{x}_{LE} - \mathbf{x})/U(x) + r/c_0$, where \mathbf{x}_{LE} is the coordinate of the airfoil leading-edge, and the dashed line depicts r/c_0 only. The position of the maximum values of

$R_{v,p}$ along x are marked by red dots. For $x/c > 0.3$ the phase shift of the $R_{v,p}$ corresponds to the group velocity $U(x)$ of the flow structures traveling the downstream distance x from the rod and cannot be attributed to the larger sound travel time from the locations \mathbf{x} to the microphone.

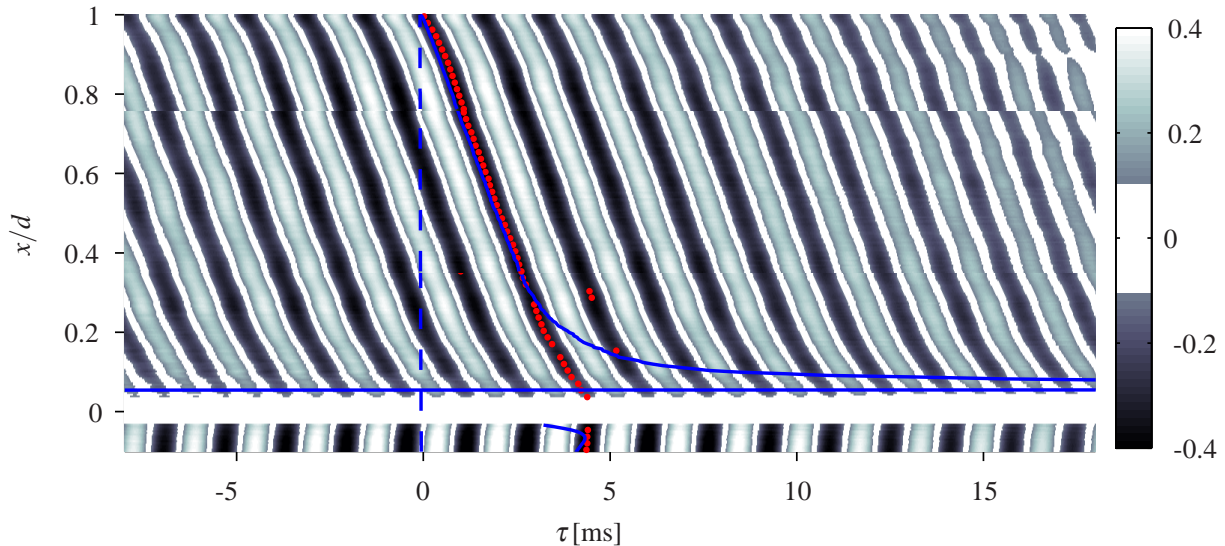


Figure 10: Temporal evolution of the normalized correlations $R_{v,p}$ along the axis $y/c = 0$. Solid line: $\tau_p(x) = (\mathbf{x}_{LE} - \mathbf{x})/U(x) + r/c_0$; dashed line: r/c_0 ; dots: $\max(R_{v,p})(x)$.

3.3 Jet

The following results have been obtained from the $Ma = 0.5$ configuration. The axes in the figures are scaled to the nozzle diameter D . In the following p are the pressure fluctuations from microphone No. 4 located at $r/D = 74$ and $\theta = 35^\circ$ (see Table 1). Two fields of view with a size of $3.89D \times 2.5D$ have been investigated. The locations of their lower left corner are $[x/D; y/D] = [2.73; -0.87]$ and $[x/D; y/D] = [6.06; -0.87]$ respectively. x , y and z are left-handed cartesian coordinates with the origin at the center of the nozzle exit. The x -axis points in the mean flow direction. A number of 8000 PIV snapshots are considered for the calculation of the cross-correlation.

In Fig. 11 $[R_{u,p}, R_{v,p}]$ is depicted as a vector field for $\tau' = -0.57$ ms. Here the retarded time $\tau' = \tau - r/c_0$ is used with $r = |\mathbf{y} - \mathbf{x}|$ where \mathbf{y} denotes the microphone position, $\mathbf{x} = [x/D; y/D] = [0; 0]$ and c_0 is the ambient sound speed. A regular pattern of vortical structures can be identified and maximum values can be observed at the core region of the jet as well as in regions outside the jet where the medium is at rest on average. It is assumed that in the outer region the acoustic particle velocity in the near-field correlates with p . The temporal evolution of $R_{v_m,p}$ is plotted in Fig. 12 for the position $[x/D; y/D] = [3.2; 0]$ in the core-region of the jet (a) and at $[x/D; y/D] = [2.87; 1.07]$ outside the jet (b). Here, v_m is the velocity component in the direction of the microphone. Note that $R_{v_m,p}$ in Fig. 12 b outside the jet has a maximum first with respect to the time delay τ' after becoming minimum, in contrast to the temporal evolution of the correlation function in the core region depicted in Fig. 12 a. The shift towards negative τ' -values cannot be attributed to the difference in sound travel time from the jet-core region to the microphones.

An explanation could be to consider the so called *lip-noise* (see [9]) as the main source of noise at the Mach-number presented here, since extrapolating the time shift from the τ' -values one would end at the nozzle position for $\tau' = 0$.

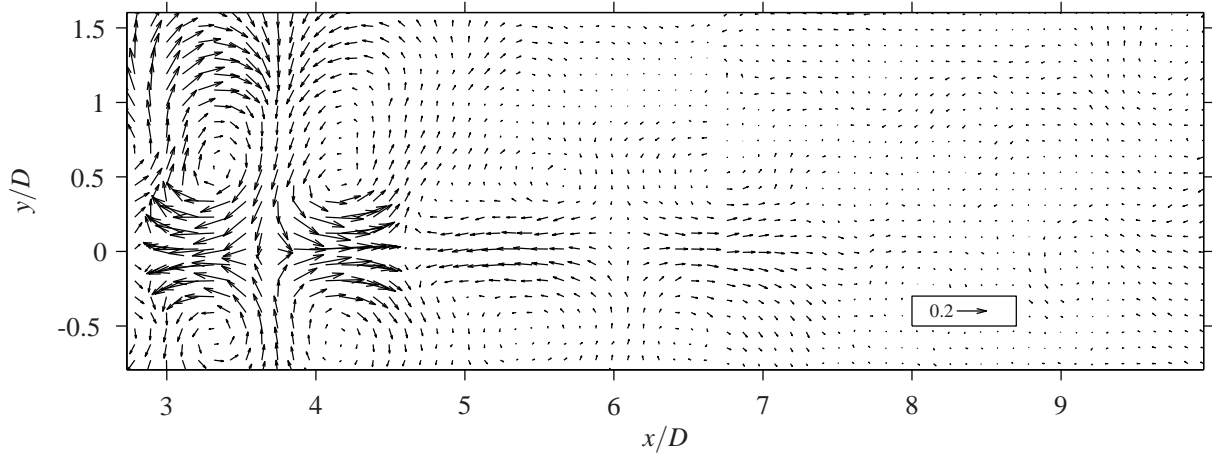


Figure 11: $[R_{u,p}, R_{v,p}]$ depicted as a vector field for $\tau' = -0.57$ ms. $\tau' = \tau - r/c_0$ with $r = |\mathbf{y} - \mathbf{x}|$.

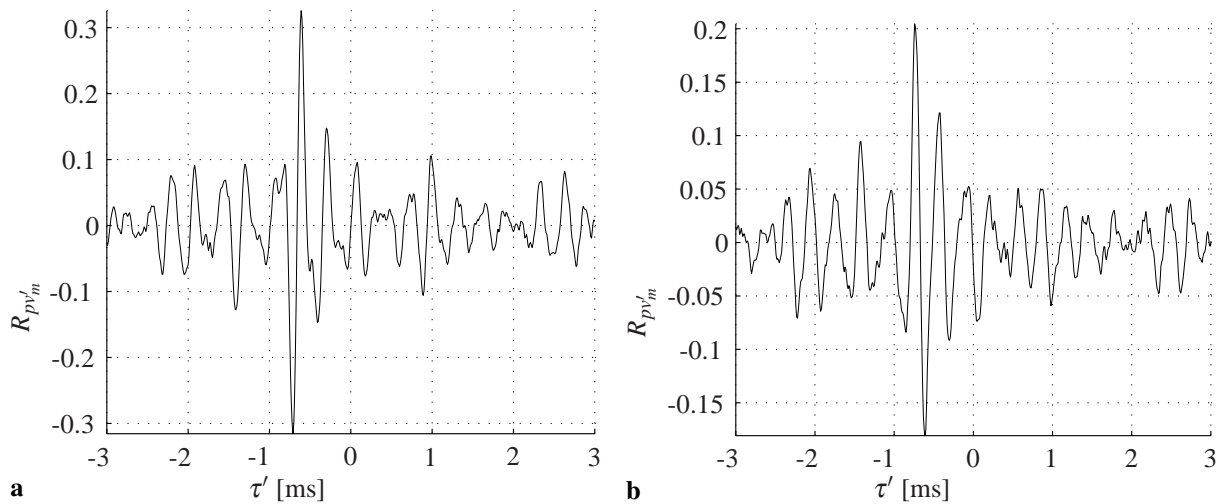


Figure 12: Temporal evolution of the cross-correlation coefficients ($R_{v_m,p}$) with τ' left: $[x/D; y/D] = [3.2; 0]$, right: $[x/D; y/D] = [2.87; 1.07]$.

4 CONCLUSION

The presented tests show that the PIV method can be used to obtain a correlation function between near-field quantities and the generated acoustic pressure. The correlation technique presented here has been successfully applied to a cylinder-wake, a rod-airfoil configuration and

cold jet. The obtained coefficient matrix provides time and space resolved information about the statistical dependency between flow structures and the acoustic pressure, even under non-anechoic conditions.

References

- [1] L. Chatellier and J. Fitzpatrick. “Spatio-temporal correlation analysis of turbulent flows using global and single-point measurements.” *Experiments in Fluids*, 38, 563 – 575, 2005.
- [2] P. J. F. Clark and H. S. Ribner. “Direct correlation of fluctuating lift with radiated sound for an airfoil in turbulent flows.” *J. Acoust. Soc. Am.*, 46(3), 802–805, 1969.
- [3] A. Henning and K. Ehrenfried. “On the accuracy of one-point and two-point statistics measured via high-speed piv.” In *14th Int. Symp. on Appl. of Laser Techn. to Fluid Mechanics. Lisbon, Portugal*. 2008.
- [4] A. Henning, L. Koop, K. Ehrenfried, A. Lauterbach, and S. Kroeber. “Simultaneous multiplane piv and microphone array measurements on a rod-airfoil configuration.” *15th AIAA/CEAS Aeroacoustics Conference, Miami, USA*, AIAA-2009-3184, 2009.
- [5] M. C. Jacob, J. Boudet, D. Casalino, and M. Michard. “A rod-airfoil experiment as benchmark for broadband noise modeling.” *Theoret. Comput. Fluid Dynamics*, 19, 171 – 196, 2005. doi:10.1007/s00162-004-0108-6.
- [6] H. K. Lee and H. S. Ribner. “Direct correlation of noise and flow of a jet.” *J. Acoust. Soc. Am.*, 52(5), 1280–1290, 1972.
- [7] J. Panda, R. G. Seasholtz, and K. A. Elam. “Investigation of noise sources in high-speed jets via correlation measurements.” *J. Fluid Mech.*, 537, 349–385, 2005.
- [8] R. Rackl and T. E. Siddon. “Causality correlation analysis of flow noise with fluid dilatation as source fluctuation.” *J. Acoust. Soc. Am.*, 65(5), 1147–1155, 1979.
- [9] D. R. Regan and W. C. Meecham. “Determination of lip noise by correlation measurements.” *The Journal of the Acoustical Society of America*, 55(S1), S73–S73, 1974. doi: 10.1121/1.1919895.
- [10] H. S. Ribner. “Quadrupole correlations governing the pattern of jet noise.” *J. Fluid Mech.*, 38(1), 1–24, 1969.
- [11] M. Schaffar. “Direct measurement of the correlation between axial in-jet velocity fluctuations and far field noise near the axis of a cold jet.” *J. Sound Vib.*, 64(1), 73–83, 1979.
- [12] T. E. Siddon. “Surface dipole strength by cross-correlation method.” *J. Acoust. Soc. Am.*, 53(2), 619–633, 1973.